

Evolution of magnetic properties and damping coefficient of Co 2 MnSi Heusler alloy with Mn/Si and Co/Mn atomic disorder

Iman Abdallah, Barthélémy Pradines, Nicolas Ratel-Ramond, Gérard Benassayag, Rémi Arras, Lionel Calmels, Jean-François Bobo, Etienne Snoeck, Nicolas Biziere

▶ **To cite this version:**

Iman Abdallah, Barthélémy Pradines, Nicolas Ratel-Ramond, Gérard Benassayag, Rémi Arras, et al.. Evolution of magnetic properties and damping coefficient of Co 2 MnSi Heusler alloy with Mn/Si and Co/Mn atomic disorder. Journal of Physics D: Applied Physics, 2017, 50 (3), pp.035003. 10.1088/1361-6463/50/3/035003 . hal-01744846

HAL Id: hal-01744846
https://hal.science/hal-01744846

Submitted on 27 Mar 2018

HAL is a multi-disciplinary open access archive for the deposit and dissemination of scientific research documents, whether they are published or not. The documents may come from teaching and research institutions in France or abroad, or from public or private research centers.

L'archive ouverte pluridisciplinaire **HAL**, est destinée au dépôt et à la diffusion de documents scientifiques de niveau recherche, publiés ou non, émanant des établissements d'enseignement et de recherche français ou étrangers, des laboratoires publics ou privés.

Evolution of magnetic properties and damping coefficient of Co_2MnSi Heusler alloy with Mn/Si and Co/Mn atomic disorder

I. Abdallah[1], B. Pradines[1], N. Ratel-Ramond[1], G. BenAssayag[1], R. Arras[1], L. Calmels[1], J.F. Bobo[1], E. Snoeck[1] and N. Biziere[1].

1. CEMES-CNRS, UPR 8011, Université de Toulouse, 29 rue Jeanne Marvig, BP 94347, 31055 Toulouse Cedex 04, France.

Abstract : Ferromagnetic resonance has been used to investigate the effect of Mn/Si and Co/Mn atomic disorder on the magnetic properties and dynamic relaxation of Co_2MnSi Heusler alloy. He^+ ion irradiation at 150 KeV is used to induce Co/Mn and Mn/Si swap in the initial structure of the material. While Mn/Si disorder is found to show similar magnetic behavior as compared to the $L2_1$ order, we observe a strong impact of Co/Mn swap on the static and dynamic properties of the alloy. These results are explained with regard to electronic band structure and damping coefficient first-principles calculations showing the modification of the minority-spin density of states at the Fermi energy and local magnetic orbital moment with Co/Mn swap.

I. Introduction

Full-Heusler alloys have become a major topic of research in magnetism in the past ten years due to their potential for spintronics and microwave devices. Indeed, some of them are predicted to be half metals [1-4] which goes along with very low microwave damping coefficient [5,6] as compared to usual ferromagnetic materials. Then, they show great potential for spin transfer torque applications as 100% spin polarization and low damping coefficient are two conditions to decrease the current density for magnetic switching [7,8]. Also, materials with low microwave energy losses are of particular interest for microwave devices such as phase lines.

Among Heusler alloys, Co_2MnSi (CMS) is particularly attractive since its high Curie temperature around 900 K [9,10] allows applications at room temperature and its damping coefficient is predicted to be among the lowest among full-Heusler [5,11]. However, these features are particularly difficult to observe experimentally. For example, only few studies report spin polarization higher than 50% at room temperature [12-14] except for two recent studies for which spin polarization above 90% has been observed by spin-resolved photoemission [15,16]. In addition, only few studies have reported a damping coefficient below 10^{-3} [16,17] for CMS with a minimum of 7×10^{-4} but for $Co_{1.9}Mn_{1.1}Si$ [16]. Otherwise, reported values are generally around or above 3×10^{-3} [18-21].

One possible reason to explain the discrepancies between the experimental and predicted values of the magnetic properties of Co_2MnSi relies on the presence of local atomic disorder. Indeed, the

magnetic properties and especially the half metallic behavior, the magnetic moment and the Gilbert damping coefficient α strongly depend on the crystal order of the material. For example, ab-initio calculations have predicted half metallicity only for the $L2_1$ and B2 order while the $D0_3$ order is supposed to show weaker magnetic moment and spin polarization [22]. However, no clear experimental evidence of the evolution of the static and dynamic properties as a function of the different class of atomic disorder has been achieved up to now.

In this work ferromagnetic resonance (FMR) is used to study the effect of Mn/Si or Co/Mn disorder on the static and dynamic magnetic parameters of the $L2_1$ order in Co_2MnSi. To achieve this goal, we recently demonstrated [23] that light He^+ ions irradiation at 150 KeV allows to induce Mn/Si and Co/Mn swaps in the $L2_1$ phase leading to regions of full B2 order and regions with $D0_3$ disorder type. Here, we demonstrate that the magnetic parameters of the B2 regions (Mn/Si disorder) are very close from the one of $L2_1$ order, except for the damping coefficient. In opposite, we show that a small amount of Co/Mn exchange induces strong and complex variations of both the static and dynamic properties of the $L2_1$ order. Electronic band structure and damping calculations including Co/Mn atomic disorder show that the experimental results can be explained by the creation of electronic states in the minority spin band at the Fermi level E_F in addition to a modification of the spin-orbit interaction due to an increase orbital moment.

II. Experimental and calculation methods

The measurements have been performed on the four samples for which a full structural characterization has been presented in Ref. [23]. First a CMS thin film has been grown by magnetron sputtering on a MgO (001) single crystal. Details about the deposition conditions are presented in Ref. [24]. The thickness of the CMS layer is 42 nm and a 10 nm MgO capping layer is deposited to avoid oxidation. This reference sample is then cut into four pieces, one as a reference and three for He^+ irradiation at 150 keV performed with a 200A2 Varian ion implanter. The irradiation is performed at room temperature and the fluences (= ions/cm²) for the three irradiated samples are 10^{15}, 5×10^{15} and 10^{16} respectively. The high kinetic energy of the ions prevents from implantation of He^+ in the CMS film as they stop several hundreds of nm deep in the substrate.

Here we summarize the main result presented in Ref [23] about the evolution of the structural properties as a function of the ion fluence. We extracted the values of the Co/Si, Mn/Si and Co/Mn atomic disorder as a function of the irradiation fluence by X-ray diffraction analysis. Also, local arrangement of atomic organization was observed by HAADF-STEM imaging. Details about the method can be found in Ref [23]. We demonstrated that the as deposited sample grows with 75% of $L2_1$ order and 25% of B2 order, this last one appearing as very small regions of few tens of nm^3 in the $L2_1$ matrix (see figure 2a in Ref. [23]). Under He^+ irradiation, the size of the regions with B2 order was shown to increase (see figure. 3a in Ref. [23]), due to Mn/Si exchange in the initial $L2_1$ matrix. In addition, the rate of Co/Si disorder was found to be small and roughly constant as a function of the

fluence, showing no influence of ion irradiation on this kind of atomic disorder. Finally, the determination of the exact value of Co/Mn disorder parameter for fluence below 10^{16} ions/cm² was difficult due to the uncertainty in the experimental procedure to extract this parameter from X-ray diffraction. We evaluate our experimental uncertainty to be around 0.02 for Co/Mn disorder. However, for a fluence of 10^{16} ions/cm², we observed a clear increase of this parameter up to 0.09, well above the experimental uncertainty. Below 10^{16} ions/cm², Co/Mn exchange was also accounted for the decrease of the magnetization amplitude measured by PPMS magnetometer and presented in figure 4. in Ref. [23]. Also, HAADF-STEM did not allow to state if Co/Mn disorder induced by irradiation appears as regions of full $D0_3$ order or if it is randomly distributed in the material.

Table 1 presents a summary of the measured disorder parameters as a function of the ion fluence. We remind that for the $L2_1$, B2, $D0_3$ and A2 crystal orders the Mn/Si, Co/Si and Co/Mn parameters are respectively equal to (0,0,0), (1/2,0,0), (0,0,2/3) and (1/4, 1/2,1/2).

Ions/cm²	REF	10^{15}	$5x10^{15}$	10^{16}
Mn/Si	0.14 ± 0.01	0.15 ± 0.01	0.20 ± 0.01	0.21 ± 0.01
Co/Si	0.02 ± 0.01	0.03 ± 0.02	0.04 ± 0.01	0.03 ± 0.01
Co/Mn	0.01 ± 0.01	0.02 ± 0.02	0.02 ± 0.02	0.09 ± 0.02

Table 1: Summary of the disorder parameters measured by X-ray diffraction and presented in figure. 1d of Ref. [23].

Broadband (0.1-30 GHz) ferromagnetic resonance in strip line geometry is used to measure the magnetic parameters of the samples. The measurement is performed at constant frequency and sweeping the external field. In order to increase the signal to noise ratio, the external magnetic field is modulated with an amplitude of 0.2 mT and a frequency of 73 Hz by two Helmholtz coils. A lock-in amplifier then measures the derivative of the microwave power absorbed by the CMS (figure 1.c). Our set-up allows for rotation of the magnetic field around the sample and then for the measurement of in plane angular dependence of the resonance fields.

Calculations of electronic band structure and damping coefficient are performed with the spin-polarized relativistic Korringa-Kohn-Rostoker (SPRKKR) code. This code is based on the KKR-Green's function formalism which uses the multiple scattering theory with periodic boundary conditions to calculate the Green's function of the system [25]. This calculation method of the electronic structure was chosen because it allows to treat random chemical disorder via the coherent potential approximation (CPA) [26]. The calculations are performed for a tetragonaly distorted unit cell containing 4 formula unit with the lattice parameters measured by X-ray and presented in Ref

[23]. For the reference sample and the one irradiated at 10^{16} ions/cm², the in plane lattice parameter is 5.63 Å while the out of plane parameter increases from 5.67 to 5.69Å. It is worth noticing that the calculations of the spin-resolved densities of states (DOS) and damping coefficient are performed at 0 K. However, as the linear response formalism chosen to calculate the Gilbert damping parameter in the SPRKKR code cannot be used for a fully ordered phase at 0 K [27], the electronic properties and the damping parameter of the $L2_1$ phase are actually calculated for a nearly $L2_1$ phase that includes a tiny 1% amount of Mn/Si atomic swaps. This is the lowest amount of disorder that can be implemented in the calculations, the DOS curves and magnetic moments of the $L2_1$ and nearly $L2_1$ phases are not distinguishable.

Moreover, the damping coefficient is evaluated considering possible electronic inter and intra band transitions. Inter-band terms account for dissipation effects resulting from transition between eigenstates whose energies vary periodically with the precession of the magnetization. Intra-band terms account for dissipation effects produced by the change during the magnetization precession of the energy of the electronic states near the Fermi level under the influence of the spin-orbit coupling. The system pushed out of its equilibrium state will create electron-hole pairs who will be annihilated by electron-lattice scattering events [28]. Other dynamic relaxation mechanisms which could increase α such magnons-magnons scattering or magnons-phonon drag are then neglected here. Then calculated values of the damping coefficient are generally much lower than reported experimental values.

III. Results

A. Reference sample

Figure. 1a presents the FMR spectra for the reference sample at 17 GHz when the external field is applied parallel to a magnetic hard axis direction. Two resonance peaks are clearly visible in agreement with the presence of B2 and $L2_1$ order, as could be expected from our X-ray diffraction and HAADF-STEM experiments in Ref [23]. The two peaks are observed for every direction of the applied magnetic field as shown by the angular dependence of the resonance fields in figure. 1b. The FMR signal is fitted with the derivative of two Lorentzian functions in order to obtain the resonance field for each peak along with their respective linewidth.

In order to recover the values of the saturation magnetization amplitude $\mu_0 M_s$, cubic anisotropy field $\mu_0 H_k$ and the gyromagnetic ratio γ of both crystal orders, the resonance frequency f_{res} Vs. $\mu_0 H_0$ and $\mu_0 H_{res}$ Vs. φ curves are fitted using the Smit-Beljer formalism [29] for which the resonance frequency is defined as:

$$\boldsymbol{f_{res} = \frac{\gamma}{M_s \sin\theta_{eq}} \left[\left(E_{\theta\theta} E_{\varphi\varphi} - E_{\theta\varphi}^{\,2} \right) \right]^{\frac{1}{2}}} \qquad (1)$$

Where θ and φ are the relative angles between the magnetization and the [001] and [110] directions of CMS respectively and θ_{eq} is the angle at equilibrium for a given amplitude of the applied field. Ms is the value of the saturation magnetization and γ is the gyromagnetic ratio. Finally, the terms into the bracket correspond to the second derivative of the free energy E with respect to θ and φ, calculated for the equilibrium positions of θ and φ.

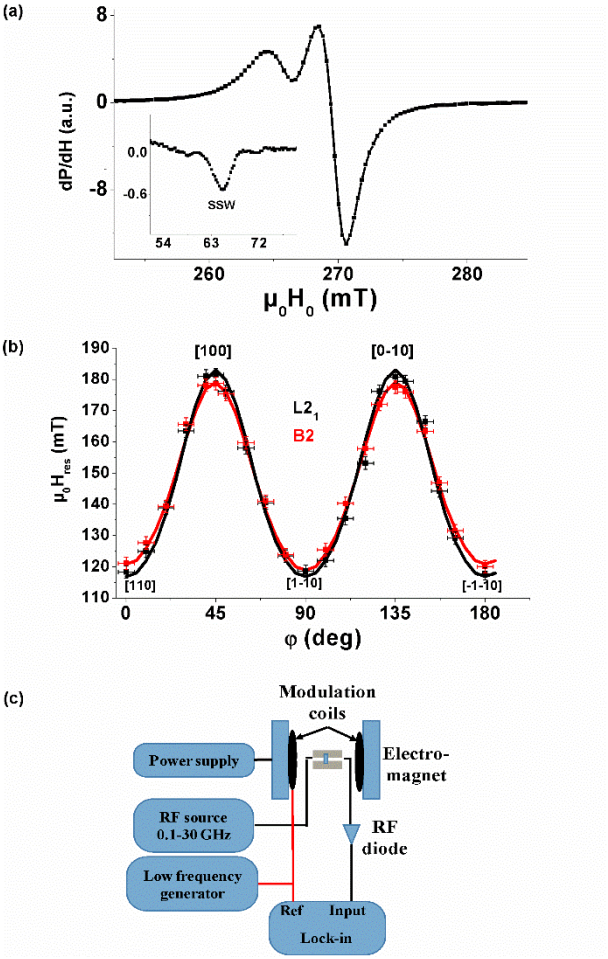


FIGURE. 1 : (a) FMR spectra of the reference sample at 17 GHz when the field is applied in the magnetic hard axis direction <100>. The symbols correspond to experimental data and the line is the fit to equation (1). The insert shows the SSW signal at low field. (b) Angular dependence of the resonance fields for the two crystal phases for the reference sample. (c) Schematic diagram of the FMR set-up. The stripline is placed at the center of the electromagnet and the sample is placed on top of the stripline. (color online)

The free energy contains all the usual magnetic contributions such as the Zeeman, cubic anisotropy, demagnetizing and exchange energies [30]. Let's note that the cubic anisotropy constant is negative in CMS [31] and then the easy magnetic axes are along the diagonals of the cubic lattice. Eq. 1 reduces in the case where the external field is applied either parallel to an easy or hard axis to:

e.a $f_{res} = \frac{\mu_0 \gamma}{2\pi}\left[(H_0 + H_k)\left(H_0 - \frac{H_k}{2} + M_s\right)\right]^{1/2}$ **(2)**

h.a $f_{res} = \frac{\mu_0 \gamma}{2\pi}[(H_0 - H_k)(H_0 - H_k + M_s)]^{1/2}$ **(3)**

The determination of the exchange constant value A is performed from the evolution with the applied field of the frequency of the first standing spin wave (SSW) mode, as shown in the insert of figure. 1a. For the SSW mode, the resonance frequencies in Eq. 2 and 3 are modified considering that H_0 transforms into $H_0 + \frac{2A}{\mu_0 M_s} k_{z,n}^2$, with $k = \pi/d$, d being the thickness of the CMS film. As the amplitude of the SSW signal is very small (about a tenth part of the FMR signal as shown in the insert of figure. 1a), only one resonance peak is measured and we attribute it to the main voluminous crystal order, i.e. the $L2_1$ order. This is in agreement with the fact that FMR is an inductive detection method, therefore sensitive to the magnetic volume.

Following this, we have extracted the values of the magnetic parameters for the reference sample. They are summarized in table II. The experimental values of the magnetic moment for the two phases are very close with corresponding moment of 4.88 and 4.85 μ_B/f.u. This is in very good agreement with the small variations of the DOS calculated for the $L2_1$ and B2 orders and presented in figure 2. The calculated total magnetic moment is 4.94 μ_B/f.u for both the $L2_1$ and B2 order, in agreement with other reported *ab initio* calculations [32-34]. We can note that magnetic moment of the bulk is not an integer unlike what would be expected. This small deviation is a result of an inherent feature of the KKR Green's function method: to calculate the Green's function, the program performs an angular momentum expansion of the wave function, which for practical reasons is limited to an integer number l_{max}. Integration leading to an integer value of the magnetic moment thus requires having $l_{max} = \infty$, which is numerically impossible [33].We also calculated the magnetic moment for an ideal cubic cell with the theoretical lattice parameter of 5.65 Å and verified that the small tetragonal distortion that we observe in our sample with respect to the perfect cubic structure has no effect on the magnetic moment amplitude (the volume of the unit cell for the reference sample is about 0.4% smaller than for the perfect cubic structure).

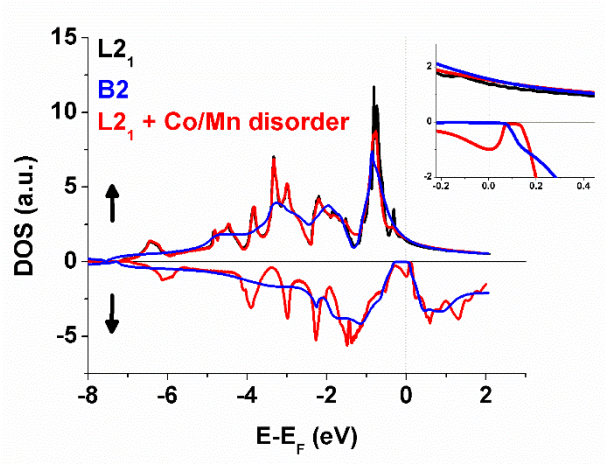


FIGURE. 2: Density of states for the perfect $L2_1$ (black) structure and for the Mn/Si (B2, blue) and Co/Mn ($D0_3$ type, red) disordered phases. (color online)

In our sample we attribute the resonance peak showing the highest magnetic moment to the $L2_1$ crystal order. This assumption is supported by the lower damping coefficient of the $L2_1$ order as compared to the B2 one in the reference sample (see below) and by the evolution of the peak positions under irradiation. This is also in agreement with the fact that the $L2_1$ peak shows the highest FMR amplitude as shown in figure 1.a. The value of the exchange constant and gyromagnetic ratio are found to be in good agreement with reported values for CMS [35-37] in the $L2_1$ order. The value of the gyromagnetic ratio leads to a Landé g factor of 2.05. While it is equal to 2 for a free electron, it is related to the spin μ_S and orbital μ_L moments in weak ferromagnet through the relation $(g-2) = 2\mu_L/\mu_S$. Therefore, the measured value of the g factor shows a small contribution from orbital moment. This is in good agreement with calculations of orbital and spin moments presented below for the $L2_1$ order. Finally, the values of the cubic anisotropy field $\mu_0 Hk$ for the $L2_1$ and B2 order are larger than usually reported ones for CMS on MgO, but similar to the one measured recently by Qiao *et al.* [17]. As crystal anisotropy finds its origin in the spin-orbit interaction, which relates the spin and orbital magnetic moment, we assume that our material shows a stronger spin-orbit coupling that in other reported studies.

We also observed differences in the values of the FMR linewidth between the two crystal orders. Figure. 3a and 3b show the linewidth ΔH as a function of the resonance frequency f_{res} in the hard and easy axes for the $L2_1$ and B2 order respectively. The Gilbert like damping coefficient α and extrinsic contribution to the linewidth ΔH_0 are extracted considering the classical approximation $\Delta H = (2\alpha/\gamma) f_{res} + \Delta H_0$. Isotropic behavior of α is observed as we measure similar values in the easy and hard axis directions, both in the $L2_1$ or B2 order. We observe the highest α value for the B2 order. While the values calculated with SPRKKR give 1.5 and 1.9×10^{-4} for the $L2_1$ and B2 order respectively, the experimental difference between the two phases is most probably to be related to the dispersed character of the B2 regions in the reference sample. Let's note that our measured value of about

1.5×10^{-3} in the $L2_1$ order is among the lowest value reported up to now. Considering that this value is overestimated due to the frequency dependent contribution of two magnons scattering [38], we can expect that the intrinsic value of α lies below 10^{-3}. However, removing the two magnons contribution implies angular in plane and out of plane linewidth measurements, but out of plane measurement is not accessible with our set-up.

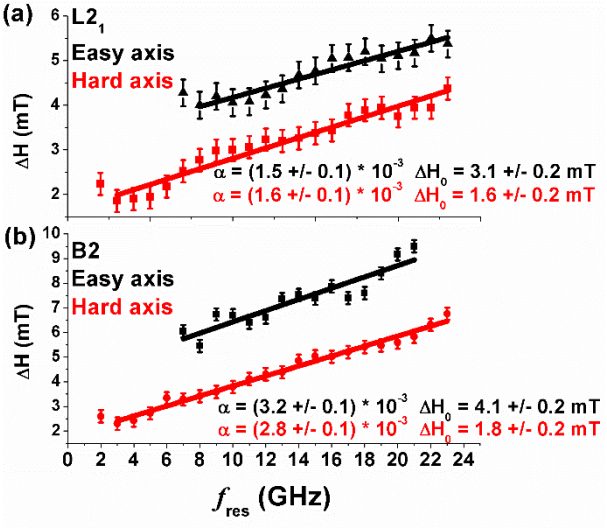


FIGURE. 3: FMR linewidth for a field applied parallel to an easy (black) or hard (red) axis direction for the $L2_1$ (a) and B2 (b) order. (color online)

At last we observe that the average extrinsic contribution to the linewidth ΔH_0, which is supposed to englobe the effect of magnetic and structural inhomogeneities in the sample, is always higher in the easy than in the hard axis direction, for both the $L2_1$ and B2 orders. While the damping coefficient α shows an isotropic behavior, the variation of ΔH_0 with the direction of the applied field leads to an anisotropic behavior of the total ΔH. We do not have clear explanation of this effect. One possibility relies on the preferential orientation of misfit dislocations along the MgO [100] directions, i.e. parallel to the [110] easy axis directions of CMS [30], which could lead to local inhomogeneity of the internal field.

B. Effect of atomic Mn/Si and Co/Mn disorder

The evolution of the FMR spectra in the hard axis direction as a function of the ion fluence is shown in figure 4.a. It is clear that the resonance peak associated to the B2 order shows roughly constant position while the one associated to the $L2_1$ order in the reference sample shifts to higher magnetic fields. The same behavior is observed for every direction of the external field.

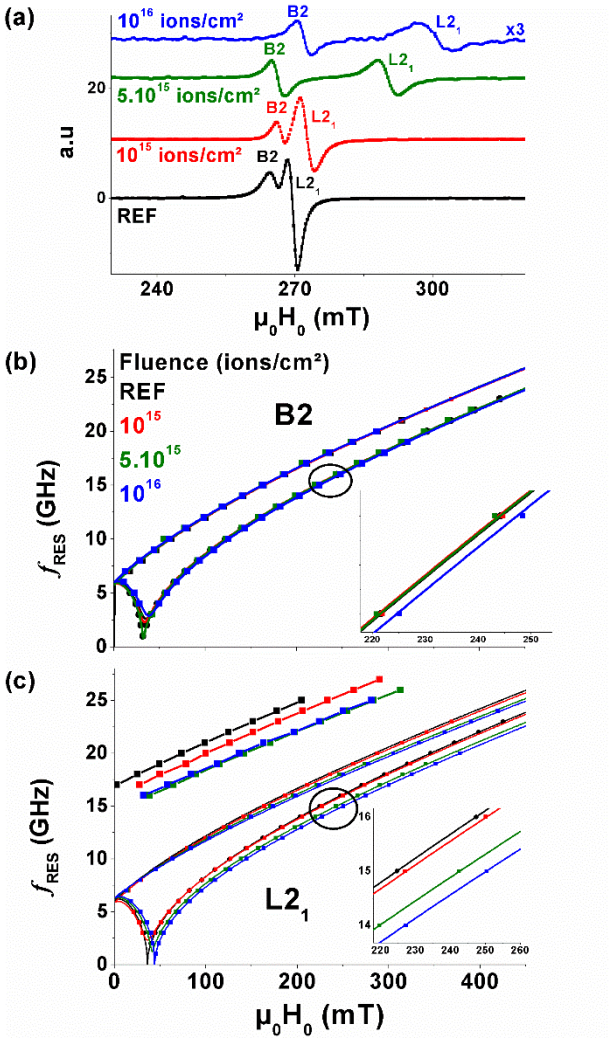


FIGURE. 4 : (a) FMR signal at 17 GHz in the hard axis direction at different fluence. The FMR signal for a fluence of 10^{16} ions/cm² is multiplied by 3 for clarity. Evolution as a function of irradiation ion fluence for the resonance frequency f_{res} Vs. the applied field $\mu_0 H_0$ for the B2 (b) and $L2_1$ (c) order respectively. (color online)

The values of magnetic parameters for each phase as a function of the fluence, extracted from the evolution of the f_{res} Vs. $\mu_0 H_0$ curves (figure 4b and c), are reported in table II. We observe that the magnetic parameters of the B2 order are not modified by ion irradiation. This confirms our structural analysis which assume that ion irradiation favors the B2 order with respect to the $L2_1$ one. This result is different from the observation of Hamrle et al. [36] who observed a decrease of the magnetic moment for fluence higher than 10^{15} ions/cm² in a B2 ordered CMS crystal irradiated with He^+ ions. However, the irradiation was performed at 30 KeV which could lead to stronger creation of local defects such as vacancies and interstitial at moderate fluence.

The constant magnetic parameters of the B2 order also mean that the Co/Mn disorder measured by X-ray does not takes place in this phase. Then it must take place only in the initial $L2_1$ matrix. As

we observe only two FMR resonance peaks even at 10^{16} ions/cm², we conclude that the Co/Mn disorder measured is randomly distributed in the initial $L2_1$ matrix. Otherwise, if region of full $D0_3$ order would be present, an additional resonance peak would be detected. Co/Mn disorder is then accounted for the variation of the magnetic parameters of the $L2_1$ order. More specifically, some parameters are found to decrease, such as the magnetization and exchange amplitude, while others are found to increase for fluence above 5×10^{15} ions/cm² such as the cubic anisotropy and gyromagnetic ratio.

In order to understand such effects, we calculated the DOS for the CMS crystal with general formula $[Co_{2-x}Mn_x][Mn_xCo_{1-x}]Si$, x being the value of Co/Mn exchange at 10^{16} ions/cm² given in table I. The terms into the first bracket are considered on the X atomic sites, the terms in the second bracket on the Y sites while the Si atoms are kept on the Z sites. Also the value of the lattice parameters at 10^{16} ions/cm² are considered in the calculation. The result of the calculation is shown in figure. 2. The first observation is the apparition of electronic states for spin down at the Fermi level, leading to a loss of the half metallicity. This is in agreement with the work of Picozzi *et al.* [22]. Our calculated value of the total magnetic moment is 4.65 μ_B, so a decrease of about 6% as compared to the bulk value. This is in qualitative agreement with the experiment even if we measure a stronger decrease of the total magnetic moment. Indeed, experimentally, it falls down to 4.26 μ_B, therefore about 12 % in the initial $L2_1$ moment. As the magnetization and exchange interaction are intrinsically related in ferromagnet, it is not surprising that we find a decreasing value of the exchange constant A. While it does not appear clearly in our DOS calculations presented in figure 2, it was demonstrated by Picozzi *et al.* that Co/Mn swap induces a shift of the energy band for the minority spin states toward lower energies, which could be seen as a decrease of the exchange splitting. Moreover, Pandey *et al.* [39] demonstrated that the exchange constant decreases when increasing the lattice parameters of a few percent. Then we assume that the decrease of exchange constant observed in our experiment is most probably due to both the increase of the out of plane lattice parameter and the presence of Co/Mn disorder.

In addition, we observe a strong increase of the anisotropy field while the value of the cubic anisotropy constant $K_c = \frac{1}{2}\mu_0 M_S H_K$ is found to be roughly constant up to 5×10^{15} ions/cm². Then, the variation of anisotropy field can be considered to come mainly from the evolution of the magnetization. Nevertheless, at 10^{16} ions/cm², we observe a small increase of K_c, meaning an increase of the spin-orbit interaction. A possible explanation of this effect is given by the calculation of the orbital and spin moment with Co/Mn swap. While the spin moment decreases from 4.87 for the $L2_1$ order to 4.57 μ_B for the disordered state, the orbital moment increases from 0.07 to 0.08 μ_B. Then we assume that the spin-orbit interaction increases due to the variation of the orbital contribution. The increase of orbital moment is also assumed to explain the increase of the gyromagnetic ratio above 5.10^{15} ions/cm² since γ is related to the Landé factor g such as $\gamma = \frac{g*|e|}{2m_e}$, with $(g-2) = 2\frac{\mu_L}{\mu_s}$. As μ_L increases and μ_s decreases with Co/Mn swap, γ increases.

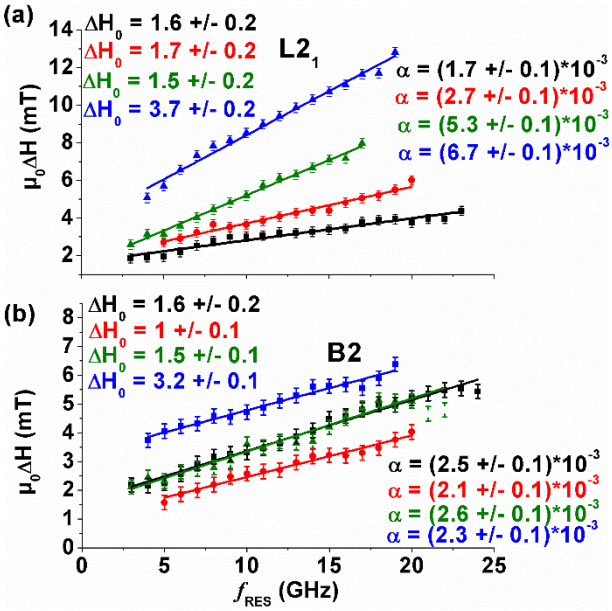


FIGURE. 5 : Evolution of the FMR linewidth in the hard axis direction as a function of the ion fluence for the $L2_1$ (a) and B2 (b) order. (color online)

Finally, we studied the evolution of the dynamic relaxation as a function of the ion fluence for each crystal order. This is presented in figure. 5 for one hard axis direction. Similar results are observed in the easy axis directions. Basically, the damping coefficient in the B2 order is found to be roughly constant, similarly to the others magnetic parameters. However, we observe some variations of the extrinsic contributions ΔH_0 as a function of the fluence. At 10^{15} ions/cm², the extrinsic contributions are found to decrease. This may be related to the local improvement of the long range order in the B2 phase as stated by Hamrle *et al.* At the highest fluence however, the extrinsic contributions are found to increase as compared to the reference. This could be explained by the presence of local defects induced by the ion irradiation.

In order to give an order of magnitude of the density of vacancies in the material, we performed simulations of the CMS damage with IPROS, a homemade Monte-Carlo software for ion implantation. Results of the simulations for a fluence of 10^{16} ions/cm² are presented in figure. 6. They show the same amount of vacancies for every atoms leading to about 2% of vacancies in total (the density of CMS being about 9.10^{23} at/cm^3). However, IPROS allows to simulate only stoichiometric amorphous material and then the crystal structure and binding energies are not considered [40-42]. Furthermore, simulations are performed at 0 K and then atomic recombination at room temperature are not taken into account. Then the amount of vacancies is overestimated by IPROS and the real density of vacancies is below 2%. In order to verify the possible effect of vacancies on the damping coefficient, we have calculated α in the B2 order considering a trial value of 1% of vacuum randomly distributed over each atomic sites. We found a value of about 2.10^{-4} very close from the value of 1.9×10^{-4} for the

bulk with no defects. This calculation and the experimental measurement of α seem to show that the small amount of vacancies created by irradiation has minor effect on the damping coefficient in the B2 order but we clearly observe experimentally that the linewidth is very sensitive to a small amount of defect in the material due to the extrinsic contribution. Considering fluences lower than 10^{16} ions/cm², we believe that vacancies creation due to irradiation might be neglected. This assumption is supported by the IPROS simulations (2 vacancies maximum for 10 000 CMS atoms at 10^{14} ions/cm²) and experimentally by the similar values of ΔH_0 for a fluence of 5.10^{15} ions/cm² and for the reference sample.

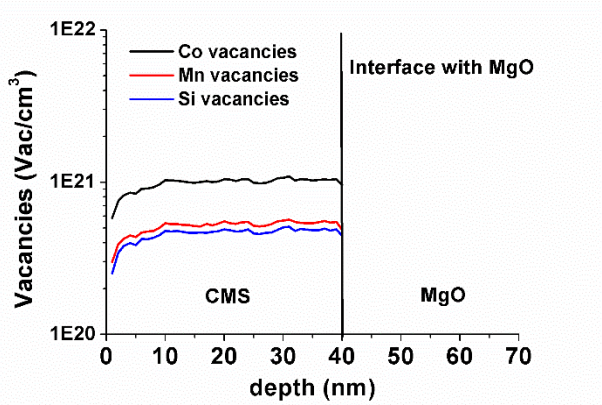


FIGURE. 6 : Density of vacancies for each atomic specie for an irradiation fluence of 10^{16} ions/cm². The density of vacancies for the Co is twice the one of Mn or Si due to the double amount of Co atoms in the unit cell. (color online)

For the $L2_1$ order, the situation is slightly different. While the extrinsic contributions are found to increase for the highest fluence as for the B2 order, we observe an increase of the damping coefficient even at low fluence. Considering the model of Kamberský for the dynamic relaxation in metals [43,44], α is proportional to the total DOS at the Fermi level. Then the increase of α with Co/Mn swap is correlated to the apparition of minority states at the Fermi level (as shown in the zoom in figure. 2) allowing for inter-band spin flip relaxation channel. The calculation of α for the $L2_1$ order including the amount of Co/Mn disorder measured at 10^{16} ions/cm² gives a value of 7.7×10^{-4} to be compared with the initial value of 1.5×10^{-4}. This strong variation is qualitatively in good agreement with the experimental observations. Let's note that we also calculated the effect of 1% of vacancies on the α value in the $L2_1$ order, again with the vacancies uniformly distributed over all atomic sites. We found that α increases up to 2×10^{-4}. If the effect of local defects is not negligible, it is much less than the effect of chemical disorder.

It is worth noticing that even if we were not able to get values of the Co/Mn exchange parameter with a precision better than 0.02 in our structural analysis, the high sensitivity of the damping to Co/Mn exchange and the experimental observation of the increase of α most probably demonstrates

that a small amount of Co/Mn disorder already takes place in the $L2_1$ phase at fluence of 10^{15} and $5x10^{15}$ ions/cm². The measurement of the damping coefficient in CMS is then a very sensitive probe of the atomic disorder.

Ions/cm²	REF	10^{15}	5 x 10^{15}	10^{16}
		$L2_1$		
$\mu_0 M_s$ (T)	1.26 ± 0.02	1.22 ± 0.02	1.14 ± 0.02	1.1 ± 0.02
$\mu_0 H_k$ (mT)	36 ± 0.5	34 ± 0.5	42 ± 0.5	45 ± 0.5
Kc (kJ/m^3)	18 +/- 0.5	17 +/- 0.5	19 +/- 0.5	19.8 +/- 0.5
γ (GHz/T)	28.7 ± 0.1	28.7 ± 0.1	28.8 ± 0.1	28.9 ± 0.1
A (pJ/m)	19 ± 0.1	18 ± 0.1	12 ± 0.1	13 ± 0.1
		B2		
$\mu_0 M_s$ (T)	1.25 ± 0.02	1.25 ± 0.02	1.25 ± 0.02	1.25 ± 0.02
$\mu_0 H_k$ (mT)	32 ± 0.5	33 ± 0.5	35 ± 0.5	36 ± 0.5
Kc (kJ/m^3)	15.9 +/- 0.5	16.4 +/- 0.5	17.4 +/- 0.5	17.9 +/- 0.5
γ (GHz/T)	28.7 ± 0.1	28.7 ± 0.1	28.7 ± 0.1	28.7 ± 0.1

TABLE II. Magnetic parameters obtained from the best fits to the experimental FMR results.

IV. Conclusion

In summary, we have investigated the effect of Mn/Si and Co/Mn atomic disorder on the magnetic properties of the CMS alloy. We demonstrated that the B2 crystal order in CMS has similar magnetic parameters than the $L2_1$ order, except for the damping coefficient which is higher, but most probably because of the local organization of this phase in our reference sample. The effect of ion irradiation for this phase is shown to only modify the extrinsic contributions to the relaxation in agreement with an increased number of defects. From a fundamental point of view this method may be interesting to study in detail the role of local defects on magnons-magnons relaxation processes.

In opposite, we clearly demonstrated that very low concentration of Co/Mn swap in the $L2_1$ order is sufficient to change drastically the magnetic properties of the CMS. While the creation of additional states at E_F for the minority spins explains the variation of the magnetization and damping, the calculated increase of the orbital magnetic moment with Co/Mn swap is assumed to explain the increased gyromagnetic ratio and the variation of the cubic anisotropy in relation with the spin-orbit interaction.

Acknowledgment

This work has been supported by the French Agence Nationale pour la Recherche (ANR NASSICS 12-JS10-00801) and the French Labex NEXT (HEUMAC). This work was granted access to the HPC resources of CALMIP supercomputing center under the allocation 2016-p1252 and 2016-p1554.

References

[1] R. A. De Groot, F. M. Mueller, P. G. Van Engen, and K. H. J. Buschow, Phys. Rev. Lett., vol. 50, no. 25, pp. 2024–2027, 1983.

[2] I. Galanakis, P. H. Dederichs, and N. Papanikolaou, Phys. Rev. B, vol. 66, 17, 174429, 2002.

[3] I Galanakis, Ph. Mavropoulos and P H Dederichs, J. Phys. D: Appl. Phys. 39, 765–775, 2006.

[4] S. Ishida, S. Fujii, S. Kashiwagi and S. Asano, Journ. of the Physical Society of Japan, 64, 2152, 1995.

[5] C. Liu, C. K. A. Mewes, M. Chshiev, T. Mewes, and W. H. Butler, Appl. Phys. Lett., 95, 022509, 2009.

[6] A. Sakuma, J. Phys. D: Appl. Phys. 48, 164011 (2015).

[7] P. Buczek, A. Ernst, P. Bruno, and L.M. Sandratskii, Phys. Rev.Lett. 102, 247206, (2009).

[8] M. Tsoi, A. G. M. Jansen, J. Bass, W. C. Chiang, V. Tsoi, and P.Wyder, Nature, 406, 46, (2000).

[9] J. A. Katine, F. J. Albert, R. A. Buhrman, E. B. Myers, and D. C. Ralph, Phys. Rev. Lett. 84, 3149, 2000.

[10] P. J. Webster, J. Phys. Chem. Solids, 32, 1221, 1971.

[11] P. J. Brown, K. U. Neumann, P. J. Webster, and K. R. A. Ziebeck, J. Phys. Condens. Matter, 12, 1827, 2000.

[12] Y. Sakuraba, M. Hattori, M. Oogane, Y. Ando, H. Kato, A. Sakuma, T. Miyazaki, and H. Kubota, Appl. Phys. Lett. 88, 192508, (2006).

[13] J. Schmalhorst, A. Thomas, S. Kämmerer, O. Schebaum, D. Ebke, M. D. Sacher, G. Reiss, A. Hütten, A. Turchanin, A. Gölzhäuser and E. Arenholz, Phys. Rev. B 75, 014403 (2007).

[14] H. Liu, Y. Honda, T. Taira, K. Matsuda, M. Arita, T. Uemura, and M. Yamamoto, Appl. Phys. Lett. 101, 132418 (2012).

[15] M. Jourdan, J. Minar, J. Braun, A. Kronenberg, S. Chadov, B. Balke, A. Gloskovskii, M. Kolbe1, H.J. Elmers, G. Schonhense, H. Ebert, C. Felser4 & M. Klaui, Nat. Com. 5, 3974, 2014.

[16] S. Andrieu, A. Neggache, T.Hauet, T. Devolder, A. Hallal, M. Chshiev, A. Bataille, P. Lefevre, F. Bertran, Phys. Rev B. 93, 094417 (2016).

[17] S.-Z. Qiao, J. Zhang, Y.-F. Qin, R.-R. Hao, H. Zhong, D.-P. Zhu, Y. Kang, S.-S. Kang, S.-Y. Yu, G.-B. Han, S.-S. Yan, and L.-M. Mei, Chin. Phys. Lett., 32, 057601 (2015).

[18] F. J. Yang and X. Q. Chen, Applied Physics Letters 102, 252407 (2013).

[19] T. Kubota, S. Tsunegi, M. Oogane, S. Mizukami, T. Miyazaki, H. Naganuma, and Y. Ando, Appl. Phys. Lett., 94, 122504 (2009).

[20] R. Yilgin, M. Oogane, Y. Ando, and T. Miyazaki, J. Magn. Magn. Mater., 310, 2322 (2007).

[21] M Oogane, T Kubota, H Naganuma and Y Ando, J. Phys. D: Appl. Phys., 48, 164012 (2015).

[22] S. Picozzi, A. Continenza, A. J. Freeman, Phys. Rev. B., 69, 094423 (2004).

[23] I. Abdallah1, N. Ratel-Ramond, C. Magen, B. Pecassou, R. Cours, A. Arnoult, M. Respaud, J.F. Bobo, G. BenAssayag, E. Snoeck and N. Biziere, Mater. Res. Express 3, 046101 (2016).

[24] G. Ortiz, A. Garcia, J. BenYoussef, N. Biziere, F. Boust, J.F. Bobo, E. Snoeck and N. Vukadinovic, IEEE Trans. Mag., 49, 3 (2013).

[25] H. Ebert, D. Kdderitzsch, and J. Minr, Reports on Progress in Physics 74, 096501 (2011).

[26] P. Soven, Physical Review, 156, 809 (1967).

[27] A. Kohler, L. Wollmann, D. Ebke, S. Chadov, C. Kaiser, Z. Diao, Y. Zheng, Q. Leng, C. Felser, Phys. Rev. B., 93, 094410 (2016).

[28] V. Kamberský Czech. Jour. of Phys. B., 26, 1366 (1976).

[29] Smit, J. and H.G. Belgers, Philips Res. Rep., 10, 113 (1955).

[30] G. Ortiz, A. Garcıa-Garcıa, N. Biziere, F. Boust, J. F. Bobo and E. Snoeck, Jour. of Appl. Phys., 113, 043921 (2013).

[31] S. Trudel, O. Gaier, J. Hamrle and B. Hillebrands, J. Phys. D: Appl. Phys. 43, 193001 (2010).

[32] S. Fujii, S. Sugimura, Ishida, and S. Asano, Jour. of Phys. : Cond. Matt., 2, 8583 (1990).

[33] I. Galanakis, P. H. Dederichs, and N. Papanikolaou, Phys. Rev. B., 66, 174429 (2002).

[34] G. H. Fecher, D. Ebke, S. Ouardi, S. Agrestini, C.-Y. Kuo, N. Hollmann, Z. Hu, A. Gloskovskii, F. Yakhou, N. B. Brookes and C. Felser, SPIN 04, 1440017 (2014).

[35] L. Ritchie, G. Xiao, Y. Ji, T. Y. Chen, C. L. Chien, M. Zhang, J. Chen, Z. Liu, G. Wu, and X. X. Zhang, Phys. Rev. B, 68,104430 (2003).

[36] J. Hamrle, O. Gaier, S.G. Min, B. Hillebrands, Y. Sakuraba and Y Ando, Jour. of Phys. D : Applied Physics, 42, 084005 (2009).

[37] *B. Rameev et al., Physica Status Solidi (a), 203,1503(2006).*

[38] M. Belmeguenai, H. Tuzcuoglu, M. S. Gabor, T. Petrisor Jr., C. Tiusan, D. Berling, F. Zighem, T. Chauveau, S. M. Cherif, and P. Moch, Phys. Rev. B., 87, 184431 (2013).

[39] H. Pandey, P. C. Joshi, R. P. Pant, R. Prasad, S. Auluck and R. C. Budhani, Jour. of Appl. Phys., 111, 023912 (2012).

[40] J. Ziegler, J. Biersack and U. Littmark, The Stopping of Ions in Matter, ed. Pergamon, New York, (1985).

[41] Vacancies and Interstitials in Metals, ed. A. Seeger, D. Schumacher, W. Schilling and J. Diehl, North Holland, Amsterdam (1970).
[42] H. Bernas, J.-P. Attane, K.H. Heinig, D. Halley, D. Ravelososa, A. Marty, P. Auric, C. Chappert, Y. Samson, Phys. Rev. Lett. 91, 077203 (2003).
[43] J. Pelzl, R. Meckenstock, D. Spoddig, F. Schreiber, J. Pflaum and Z. Frait, J. Phys.: Condens. Matter 15, S451 (2003).
[44] V. Kambersky, Can. J. Phys. B 26**,** 2906 (1970).